

Theory of liquid film growth and wetting instabilities on graphene

Sanghita Sengupta,^{1,2} Nathan S. Nichols,^{1,2} Adrian Del Maestro,^{1,2,3} and Valeri N. Kotov^{1,2}

¹*Department of Physics, University of Vermont, Burlington, VT 05405*

²*Materials Science Program, University of Vermont, Burlington, VT 05405*

³*Institut für Theoretische Physik, Universität Leipzig, D-04103, Leipzig, Germany*

We investigate wetting phenomena near graphene within the Dzyaloshinskii-Lifshitz-Pitaevskii theory for light gases of hydrogen, helium and nitrogen in three different geometries where graphene is either affixed to an insulating substrate, submerged or suspended. We find that the presence of graphene has a significant effect in all configurations. When placed on a substrate, the polarizability of graphene can increase the strength of the total van der Waals force by a factor of two near the surface, enhancing the propensity towards wetting. In a suspended geometry unique to two-dimensional materials where graphene is able to wet on only one side, liquid film growth becomes arrested at a critical thickness which may trigger surface instabilities and pattern formation analogous to spinodal dewetting. The existence of a mesoscopic critical film with a tunable thickness provides a platform for the study of a continuous wetting transition as well as engineering custom liquid coatings. These phenomena are robust to some mechanical deformations and are also universally present in doped graphene and other two-dimensional materials, such as monolayer dichalcogenides.

The wetting of an electrically neutral solid surface by a liquid is controlled by the relative size of attractive van der Waals interactions between molecules in the liquid and those between the liquid and substrate. For weak liquid-substrate interactions, the surface may undergo *partial wetting* manifest as the coexistence of distinct liquid droplets with an atomically thin layer of adsorbed molecules between them. In the opposite *complete wetting* regime, the liquid atoms are strongly attracted to the surface resulting in the formation of a macroscopically thick film in equilibrium with the vapor above it [1].

The growth and stability of this film beyond a few atomic layers is dominated by the long range *tail* of the van der Waals (vdW) interaction which can be thought of as creating an effective repulsion between the liquid-vapor and liquid-substrate boundaries [2–4]. For intermediate liquid-surface interactions it is possible that at a critical film thickness, d_c , (larger than any atomic length scale) this repulsion vanishes and wetting is arrested due to the lack of any energetic gain for molecules in the vapor to adsorb into the liquid – a scenario known as *incomplete wetting* [1, 5–7].

While a phase transition between partial and complete wetting driven by temperature is generically first order (being controlled by short-distance details of the adsorption potential) a transition from incomplete to complete wetting can be continuous due to the presence of only long range vdW forces [8, 9] (critical wetting). However, engineering substrates with weak interactions to observe incomplete wetting and any associated critical phenomena has been challenging, with experiments concentrating on quantum fluids at low temperatures [10, 11] or liquid substrates such as alkynes on water at high temperature [12–14].

In this letter we report on the physics of wetting in the novel class of geometries depicted in Fig. 1, made

possible by the ability to readily fabricate and manipulate atomically flat two-dimensional (2D) crystals such as graphene [15], transition-metal dichalcogenides [16] (*e.g.* MoS₂) and representatives of the 2D topological insulator family [17–20] (silicene and germanene). This includes graphene placed on a substrate, submerged in a liquid, or suspended with a vacuum underneath, realizable due to the impermeability of graphene to even small atoms [21, 22].

We devise an extension of the Dzyaloshinskii-Lifshitz-Pitaevskii (DLP) theory [2, 3] (the standard many-body approach used for accurate analysis of experiments [23, 24]) to include the polarization of a 2D material in an anisotropic layered dielectric sandwich. The results indicate that light gases near suspended 2D materials are an ideal system to study and characterize critical wetting phenomena. Our main findings include: (I) the presence of graphene on a substrate can enhance liquid film growth consistent with studies of its “partial wetting transparency” to liquid water [25]. (II) This effect rapidly decreases with film thickness and occurs at nm scales as opposed to the μm distances where relativistic effects may become important [26]. (III) In the suspended geometry, the existence of vacuum beneath graphene causes incomplete wetting with a critical film thickness on the order of 3 to 50 nm that can be tuned through the dynamic polarizability of the adsorbant or the properties of the semimetal (*e.g.* strain). This phenomenon is universally present, and can be additionally controlled in doped graphene as well as in insulating dichalcogenides, thus spanning a wide range of 2D Dirac materials. (IV) The mesoscopic film may exhibit critical surface instabilities including pattern formation in analogy to spinodal decomposition [27–33]. Together these findings represent not only the introduction of a new platform for the study of wetting and associated critical phenomena, but hint at applications including the creation of tunable surface

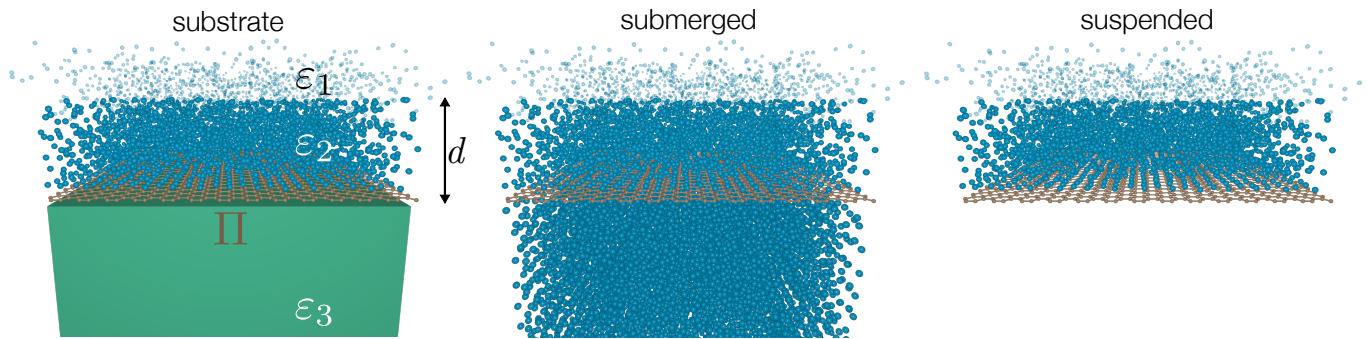


FIG. 1. Three geometries that are unique to wetting on two-dimensional materials. From left to right – Substrate: graphene with a momentum and frequency dependent electronic polarization $\Pi(\mathbf{q}, i\omega)$ is placed on top of an insulating substrate with dielectric constant ε_3 and a macroscopic liquid film with ε_2 grows to a thickness d that is in equilibrium with its vapor ($\varepsilon_1 \approx 1$). Submerged: graphene is floated on top of a liquid with dielectric constant ε_2 and a liquid film of the same substance grows on the top side. Suspended: a liquid film grows on top of a flexible graphene sheet.

coating or drying mechanisms via electrostatic gating or mechanical manipulation.

The remainder of this paper is organized as follows: we review the DLP theory and show how it is modified by the insertion of a graphene sheet. We report quantitative results for wetting and film growth in the three configurations in Fig. 1. For the suspended geometry, we examine the spreading of droplets on the liquid surface and discuss the formation of long-wavelength surface instabilities. We conclude with a discussion of the experimental measurement of these effects. Accompanying supplemental materials (SM) provide information on the effects of temperature, different 2D materials and substrates, uniaxial strain and electronic doping [34].

The starting point is the calculation of the vdW energy $U(d)$ of a charge neutral system composed of three substances (having dielectric functions $\varepsilon_{1,2,3}$) as shown in Fig. 1, with the atomically thin graphene layer, characterized by polarization Π , inserted at the boundary between regions 2 and 3. $U(d)$ represents the vdW interaction between the 1-2 and 2-3 material surface boundaries separated by distance d . It is well-known [3, 35] that $U(d)$ can be related to the momentum (\mathbf{q}) and frequency (ω) dependent effective dielectric function $\mathcal{E}(\mathbf{q}, i\omega)$ which characterizes the screening of the interlayer Coulomb potential. $U(d) = (\hbar/n)(2\pi)^{-3} \int d^2\mathbf{q} \int_0^\infty d\omega \ln \mathcal{E}(\mathbf{q}, i\omega)$, where $n = N/V$ is the density of the liquid (material 2). It should be noted that for a single-material system (i.e. characterized by only one dielectric constant) this formula is simply the random phase approximation (RPA) correlation energy, while in the case of anisotropic layered structures it represents the fluctuation (vdW) energy. We set $\hbar = 1$ from now on.

The calculation of \mathcal{E} involves the electrostatics of a three layer system. For example, for the configurations of interest in Fig. 1 one obtains the following formula [36, 37] for the properly screened interlayer Coulomb

potential U_{12} between 1 and 2: $U_{12} = V_{12}/\varepsilon_g$, $V_{12} = 8\pi e^2 \varepsilon_2 / [qD(q)]$, where $q = |\mathbf{q}|$ is the magnitude of the in-plane momentum,

$$D(q) = (\varepsilon_1 + \varepsilon_2)(\varepsilon_2 + \varepsilon_3)e^{qd} + (\varepsilon_1 - \varepsilon_2)(\varepsilon_2 - \varepsilon_3)e^{-qd} \quad (1)$$

and the effect of graphene is in the additional screening characterized by

$$\varepsilon_g(\mathbf{q}, i\omega) = 1 - V_2(q)\Pi(\mathbf{q}, i\omega). \quad (2)$$

Here, V_2 is the Coulomb potential within the lower boundary plane

$$V_2 = \frac{4\pi e^2}{qD(q)} [(\varepsilon_1 + \varepsilon_2)e^{qd} + (\varepsilon_2 - \varepsilon_1)e^{-qd}]. \quad (3)$$

The polarization of graphene $\Pi(\mathbf{q}, i\omega)$ is described in the SM [34, 38]. Then, keeping in mind that $U_{12} \propto e^2 e^{-qd} / [q\mathcal{E}(\mathbf{q}, i\omega)]$, we obtain $\mathcal{E}(\mathbf{q}, i\omega) = \varepsilon_g(\mathbf{q}, i\omega)D(q)e^{-qd}$, and finally

$$U(d) = \frac{1}{n(2\pi)^3} \int d^2\mathbf{q} \int_0^\infty d\omega \ln [\varepsilon_g(\mathbf{q}, i\omega)D(q)e^{-qd}]. \quad (4)$$

It is instructive to simplify Eq. (4) in the limit $(\varepsilon_2 - 1) \ll 1$, which is satisfied with high accuracy for the low-density systems we have studied (such as He and other light elements). In this case, their vapor can be considered as vacuum ($\varepsilon_1 = 1$), and suppressing \mathbf{q} and ω dependence:

$$U(d) \approx \frac{1}{n(2\pi)^3} \int d^2\mathbf{q} \int_0^\infty d\omega (\mathcal{U}_d + \mathcal{U}_g), \quad (5)$$

with dielectric:

$$\mathcal{U}_d = \frac{(\varepsilon_2 - 1)(\varepsilon_3 - \varepsilon_2)}{(\varepsilon_2 + 1)(\varepsilon_3 + \varepsilon_2)} e^{-2qd} \quad (6)$$

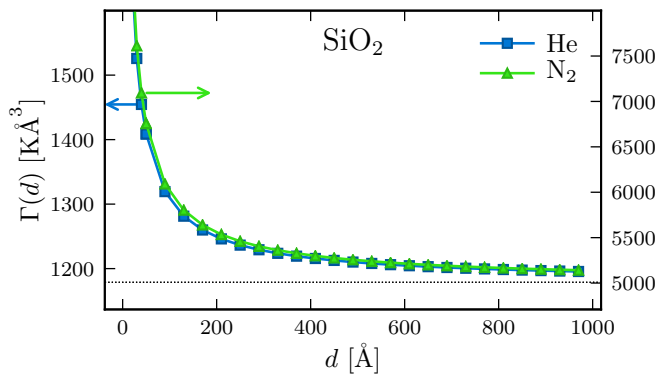


FIG. 2. Additional liquid film thickness dependence $\Gamma(d)$ (beyond $1/d^3$) of the van der Waals force between the substrate-liquid and liquid-vapor interfaces due to the insertion of graphene on a SiO_2 substrate. The dashed line represents the substrate contribution (in the absence of graphene) and a crossover from $1/d^4$ to $1/d^3$ is observed. Left vertical scale corresponds to helium and the right to nitrogen films.

and graphene parts:

$$\mathcal{U}_g = \frac{\left(\frac{-4\pi e^2 \Pi}{q(\varepsilon_2 + \varepsilon_3)}\right) \left(\frac{\varepsilon_2 - 1}{\varepsilon_2 + 1}\right) \left(\frac{2\varepsilon_2}{\varepsilon_2 + \varepsilon_3}\right)}{1 - \frac{4\pi e^2 \Pi}{q(\varepsilon_2 + \varepsilon_3)}} e^{-2qd}. \quad (7)$$

The corresponding vdW force can be obtained from $F(d) = -\partial U(d)/\partial d$ which has dimensions of energy due to the normalization factors chosen in Eq. (4).

When graphene is absent ($\mathcal{U}_g = 0$), we recover the well known DLP theory expression [2, 4, 39]. In particular it describes the important property of vdW repulsion (a force per unit area known as the disjoining pressure) for $(\varepsilon_3 - \varepsilon_2) > 0$. We note that inserting graphene will always lead to repulsion as $\Pi < 0$. Eq. (7) can be used to describe the three main configurations: graphene on a substrate (characterized by ε_3), submerged ($\varepsilon_3 = \varepsilon_2$), and suspended graphene ($\varepsilon_3 = 1$).

To calculate \mathcal{U}_d , we take the dielectric function of light elements to have a single oscillator form: $\varepsilon_2(i\omega) = 1 + C_A/[1 + (\omega/\omega_A)^2]$, where for ^4He we use $\omega_A = \omega_{\text{He}} \approx 27 \text{ eV}$ and $C_{\text{He}} = 0.054$. Parameters for other materials are given in the SM [34]. The substrate dielectric function can typically be well fitted to the form [40], $\varepsilon_3(i\omega) = 1 + C_{IR}/[1 + (\omega/\omega_{IR})^2] + C_{UV}/[1 + (\omega/\omega_{UV})^2]$. For example in the case of SiO_2 (quartz): $\omega_{UV} \approx 13.37 \text{ eV}$, $\omega_{IR} \approx 0.138 \text{ eV}$, and $C_{IR} = 1.93$, $C_{UV} = 1.359$. Other cases are studied in the SM [34].

The final result can be conveniently written as:

$$F(d) = \frac{\omega_A}{n16\pi^2} \frac{I(d)}{d^3} \equiv \frac{\Gamma(d)}{d^3}, \quad (8)$$

where the dimensionless expression for $I(d)$ is given in the SM [34] and is used to calculate $\Gamma(d)$. It is clear from Eqs. (5)–(7) that the dielectric part leads to a pure

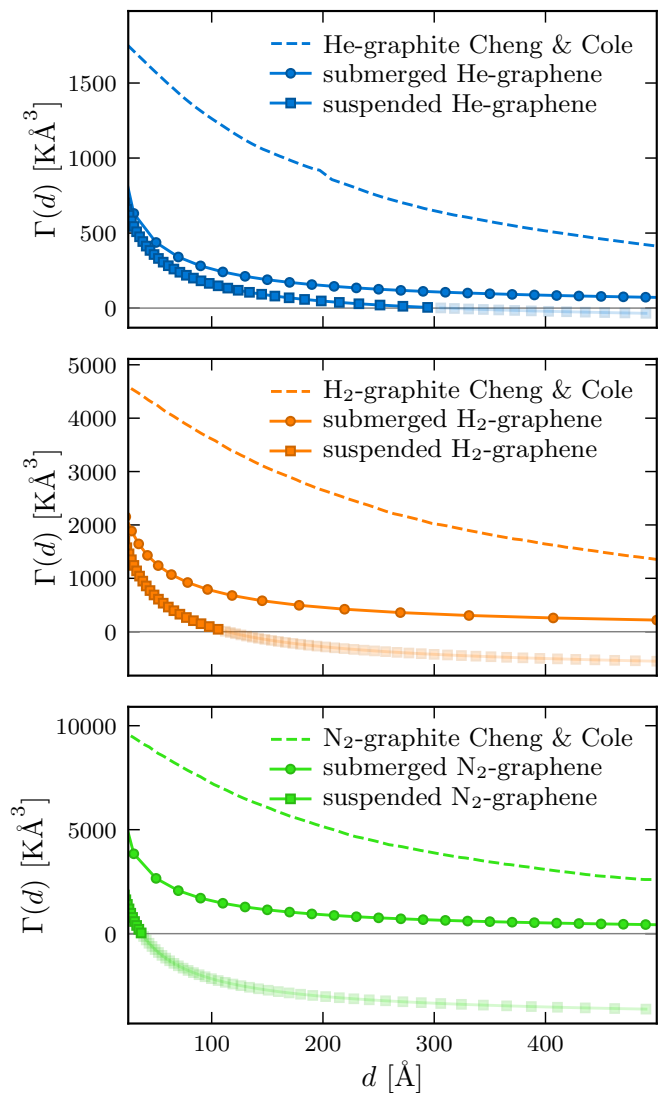


FIG. 3. Thickness dependence of the van der Waals interaction $\Gamma(d)$ for films formed on submerged and suspended graphene (see Fig. 1) composed of helium, hydrogen and nitrogen. The dashed line corresponds to films on graphite taken from Cheng and Cole [26]. For submerged graphene, $\Gamma(d \rightarrow \infty) = 0$ and in the suspended geometry, there is an instability causing film growth to be arrested where $\Gamma(d \geq d_c) \leq 0$.

$1/d^3$ dependence of the force ($\Gamma(d) = \Gamma_0$ as $\varepsilon_{1,2,3}$ do not depend on momentum). However, the graphene contribution has substantial momentum dependence (due to the polarization $\Pi(\mathbf{q}, i\omega)$), and causes a $1/d^4$ law above some length-scale. The overall behavior has the scaling form (second term due to graphene):

$$\Gamma(d) = \Gamma_0 + \frac{\Gamma_1}{d + L}. \quad (9)$$

Fig. 2 shows how the insertion of graphene on a quartz substrate enhances the vdW repulsion between

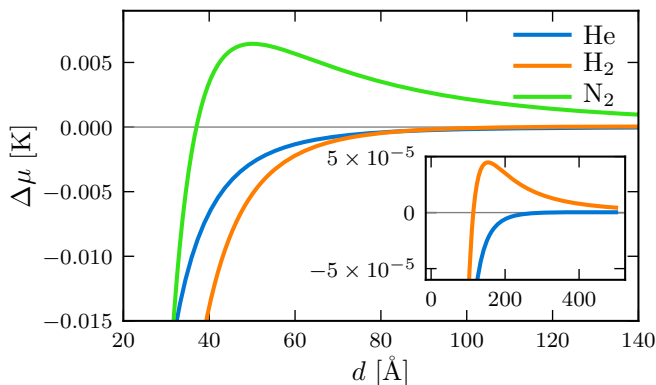


FIG. 4. Chemical potential of the liquid film (in reference to the bulk) $\Delta\mu$ as a function of distance d for suspended graphene. An instability corresponding to $\Delta\mu > 0$ is found for helium, hydrogen and nitrogen at a finite value of $d = d_c$. Inset: zoomed in region of the main panel showing d_c for He and H_2 . Values of d_c are reported in Table I.

the substrate-liquid and liquid-gas interfaces for helium and nitrogen gas. Graphene introduces a substantial distance dependence to the force that is larger than that previously reported for graphite [26, 41]. While relativistic corrections can create crossovers in the distance dependence [26], they happen at larger micron-scales, while here we see a dominant, purely non-relativistic contribution at nanometer lengths. Similar behavior is observed for other substrates such as 6H-SiC (see SM [34]). The crossover length L introduced in Eq. (9) is also sensitive to the details of the substrate and for helium we find that $L \sim 10 \text{ \AA}$, *i.e.* the crossover toward pure $1/d^4$ behavior in the graphene part occurs quite rapidly.

The vdW force in the submerged and suspended geometries that are unique to 2D materials can also be evaluated with the results shown in Fig. 3 for helium, hydrogen and nitrogen films. In all cases we compare with calculations from Cheng and Cole [26] for adsorption on graphite (dashed lines). For submerged graphene ($\varepsilon_3 = \varepsilon_2$, filled circles) $\mathcal{U}_d = 0$ (see Eq. (6)) and $\Gamma(d)$ decays to zero, in stark contrast to the case of a graphene plated substrate. For suspended graphene ($\varepsilon_3 = 1$, squares), we observe a novel physical effect for all elements: there is a critical distance d_c at which graphene’s (always positive) contribution becomes so weak it can no longer compensate the negative dielectric part and $\Gamma(d_c) = 0$. Such an effect is only possible for purely 2D materials that can be suspended without a supporting substrate - graphene [21, 42, 43] is the best (but not only) candidate in this family. For $d > d_c$ the liquid film growth stops under equilibrium conditions and the system becomes unstable. This is the incomplete wetting scenario discussed in the introduction. For $d < d_c$ the characteristic isotherms that determine the change of the chemical potential of the film (relative to bulk),

Atom	He	H ₂	N ₂
d_c (Å)	300	120	35
θ (°)	0.33	0.83	2.41

TABLE I. Critical film thickness and contact angles for three elements. The surface tensions were taken to be: $\sigma_{He} \simeq 0.26 \text{ mN/m}$, $T = 2.5 \text{ K}$; $\sigma_{H_2} \simeq 2 \text{ mN/m}$, $T = 20 \text{ K}$; $\sigma_{N_2} \simeq 10 \text{ mN/m}$, $T = 70 \text{ K}$.

$\Delta\mu = \mu(d) - \mu(d = \infty)$, are determined by the usual equilibrium condition (where P_0 is the saturated vapor pressure) [23, 44]

$$\Delta\mu = -\frac{\Gamma(d)}{d^3} = T \ln \frac{P}{P_0}, \quad P \leq P_0. \quad (10)$$

Fig. 4 shows the resulting chemical potential for helium, hydrogen and nitrogen on suspended graphene which exhibits textbook behavior [44] for an unstable system. The suspended film transition from stable ($d < d_c$) through a metastable region with $d > d_c$ where $\partial\Delta\mu/\partial d > 0$; and finally becomes unstable for $d > d_c$, $\partial\Delta\mu/\partial d < 0$. The values of the critical film thickness d_c are found to be on the order of 3 to 30 nm and are reported in Table I.

We now concentrate on the properties and implications of the incomplete wetting scenario where a liquid film with thickness d_c is absorbed on suspended graphene. As processes governing the further wetting (partial or complete) of the liquid surface are governed only by the long range tail of the vdW interaction, they can display a wealth of phenomena of both theoretical and experimental importance [1, 6, 7, 9, 10, 14, 21, 22, 45–50]. We can formulate an important question regarding wetting of the liquid film via a calculation of the contact angle θ of droplets which can form its surface. As these droplets are “far” from the substrate, the short-range adsorption potential is irrelevant, opening up the possibility of universal and continuous critical behavior. The value of the contact angle is related to the area under the $\Delta\mu(d > d_c)$ curve [2]:

$$1 - \cos(\theta) = \frac{n}{\sigma_{l-v}} \int_{d_c}^{\infty} \Delta\mu(l) dl = -\frac{n}{\sigma_{l-v}} \int_{d_c}^{\infty} \frac{\Gamma(l)}{l^3} dl \quad (11)$$

where σ_{l-v} is the liquid-vapor surface tension. Results are shown in Table I and we find small angles on the order of a degree that increase with the polarizability of the adsorbant vapor. The fact that $\theta > 0$ in all cases allows us to consider a remarkable analogy between surface film instabilities and the theory of spinodal decomposition [27–33]. The characteristic pattern instability length scale is governed by the competition between destabilizing vdW forces and the stabilizing action of the surface tension. The wavelength λ which corresponds to amplified surface fluctuations (which could ultimately cause “spinodal

dewetting”) in the unstable region ($\partial\Delta\mu/\partial d < 0$) is given by (for $d \gg L$)

$$\lambda^2 \simeq -8\pi^2 \frac{\sigma_{l-v}}{n \left(\frac{\partial\Delta\mu}{\partial d} \right)} \approx \frac{8\pi^2}{3} \frac{\sigma_{l-v} d^4}{n |\Gamma_0|}. \quad (12)$$

From Fig. 3, for example for H_2 we can estimate $|\Gamma_0| \sim 10^3 \text{ K}\text{\AA}^3$, which yields $\lambda \sim 10^4 - 10^5 \text{ \AA}$ for $d \approx 150 - 300 \text{ \AA}$.

In conclusion we have considered how the relatively weak van der Waals interactions between light atoms and graphene can substantially affect their wetting behavior when graphene is placed on a substrate, submerged in a liquid or suspended above vacuum. We find that placing graphene on a substrate enhances its propensity towards wetting during initial film growth which may have implications for its use as a conductive coating. For suspended graphene, the absence of any substrate material leads to an instability where film growth becomes arrested at a critical thickness. As the vapor pressure above this film is increased, droplets may form, driving surface fluctuations which can potentially have large amplitudes. It is significant that the critical film thickness d_c is dependent on mechanical deformations (e.g. uniaxial strain) in graphene, and is also universally present for other 2D materials, such as members of the group-VI dichalcogenides family (MoS_2 , WS_2 , MoSe_2 , etc.) [34]. Quite importantly, we also find that the instability occurs in doped graphene, within a wide range of experimentally accessible carrier densities [34]. Thus we conclude that this is a universal phenomenon in suspended 2D Dirac materials, ranging from insulating monolayer dichalcogenides to semi-metallic (undoped) and doped graphene. The exact value of d_c itself, which we find to be on the order of several hundred Angstroms, depends on material characteristics such as band gap, quasiparticle velocity, strain and doping level. Experimental confirmation of these effects would involve the measurement of adsorbed film thickness using standard quartz microbalance [10, 51] or interferometry [14] techniques. The ability to electronically or mechanically manipulate free-standing atomically flat substrates opens up the possibility of producing an exotic quantum wetting phase transition driven by a non-thermal control parameter.

We acknowledge stimulating conversations with O. Sushkov, M. Cole, and P. Taborek on the general subject of van der Waals forces and wetting. N. Nichols was supported in part by the Vermont Space Grant Consortium under NASA Grant and Cooperative Agreement NNX15AP86H. A.D. acknowledges the German Science Foundation (DFG) for financial support via grant RO 2247/10-1.

-
- [1] Daniel Bonn, Jens Eggers, Joseph Indekeu, and Jacques Meunier, “Wetting and spreading,” *Rev. Mod. Phys.* **81**, 739 (2009).
 - [2] I.E. Dzyaloshinskii, E.M. Lifshitz, and L.P. Pitaevskii, “The general theory of van der Waals forces,” *Adv. in Phys.* **10**, 165 (1961).
 - [3] Yurii S. Barash and Vitalii L. Ginzburg, “Electromagnetic fluctuations in matter and molecular (Van-der-Waals) forces between them,” *Sov. Phys. Usp.* **18**, 305 (1975).
 - [4] I.E. Dzyaloshinskii, E.M. Lifshitz, and L.P. Pitaevskii, “van der Waals Forces in Liquid Films,” *Sov. Phys. JETP* **37**, 161 (1960).
 - [5] Monique Combescot, “Classification of adsorbed films,” *Phys. Rev. B* **23**, 5623 (1981).
 - [6] J. G. Dash and Rudolf Peierls, “Characteristics of adsorbed films,” *Phys. Rev. B* **25**, 5523 (1982).
 - [7] David A Huse, “Incomplete wetting by adsorbed solid films,” *Phys. Rev. B* **29**, 6985 (1984).
 - [8] S. Dietrich and M. Schick, “Critical wetting of surfaces in systems with long-range forces,” *Phys. Rev. B* **31**, 4718 (1985).
 - [9] S Dietrich and M Napiórkowski, “Analytic results for wetting transitions in the presence of van der Waals tails,” *Physical Review A* **43**, 1861–1885 (1991).
 - [10] A. D. Migone, J. Krim, J. G. Dash, and J. Suzanne, “Incomplete wetting of ^4He films on ag and au(111) surfaces,” *Phys. Rev. B* **31**, 7643 (1985).
 - [11] E. Cheng, M. W. Cole, J. Dupont-Roc, W. F. Saam, and J. Treiner, “Novel wetting behavior in quantum films,” *Rev. Mod. Phys.* **65**, 557 (1993).
 - [12] Hisao Nakanishi and Michael E. Fisher, “Multicriticality of wetting, prewetting, and surface transitions,” *Phys. Rev. Lett.* **49**, 1565 (1982).
 - [13] E. Bertrand, D. Bonn, D Broseta, H Dobbs, J.O Indekeu, J. Meunier, K Ragil, and N Shahidzadeh, “Wetting of alkanes on water,” *J. Pet. Sci. Eng.* **33**, 217 (2002).
 - [14] Salima Rafai, Daniel Bonn, Emanuel Bertrand, Jacques Meunier, Volker C. Weiss, and Joseph O. Indekeu, “Long-Range Critical Wetting: Observation of a Critical End Point,” *Phys. Rev. Lett.* **92**, 245701 (2004).
 - [15] A. H. Castro Neto, F. Guinea, N. M. R. Peres, K. S. Novoselov, and A. K. Geim, “The electronic properties of graphene,” *Rev. Mod. Phys.* **81**, 109 (2007).
 - [16] Di Xiao, Gui Bin Liu, Wanxiang Feng, Xiaodong Xu, and Wang Yao, “Coupled Spin and Valley Physics in Monolayers of MoS_2 and Other Group-VI Dichalcogenides,” *Phys. Rev. Lett.* **108**, 196802 (2012).
 - [17] M. Ezawa, “Topological phase transition and electrically tunable diamagnetism in silicene,” *Eur. Phys. J. B* **85**, 363 (2012).
 - [18] Motohiko Ezawa, “Spin-valley optical selection rule and strong circular dichroism in silicene,” *Phys. Rev. B* **86**, 161407 (2012).
 - [19] N. D. Drummond, V. Zólyomi, and V. I. Fal’ko, “Electrically tunable band gap in silicene,” *Phys. Rev. B* **85**, 075423 (2012).
 - [20] Zeyuan Ni, Qihang Liu, Kechao Tang, Jiixin Zheng, Jing Zhou, Rui Qin, Zhengxiang Gao, Dapeng Yu, and Jing Lu, “Tunable bandgap in silicene and germanene,” *Nano Lett.* **12**, 113 (2012).

- [21] J. Scott Bunch, Scott S. Verbridge, Jonathan S. Alden, Arend M. Van Der Zande, Jeevak M. Parpia, Harold G. Craighead, and Paul L. McEuen, “Impermeable atomic membranes from graphene sheets,” *Nano Lett.* **8**, 2458 (2008).
- [22] R. R. Nair, H. A. Wu, P. N. Jayaram, I. V. Grigorieva, and A. K. Geim, “Unimpeded Permeation of Water Through Helium-Leak-Tight Graphene-Based Membranes,” *Science* **335**, 442 (2012).
- [23] E. S. Sabisky and C. H. Anderson, “Verification of the Lifshitz Theory of the van der Waals Potential Using Liquid-Helium Films,” *Phys. Rev. A* **7**, 790 (1973).
- [24] V. Panella, R. Chiarello, and J. Krim, “Adequacy of the Lifshitz Theory for Certain Thin Adsorbed Films,” *Phys. Rev. Lett.* **76**, 3606–3609 (1996).
- [25] David Parobek and Haitao Liu, “Wettability of graphene,” *2D Materials* **2**, 032001 (2015).
- [26] E. Cheng and Milton W. Cole, “Retardation and many-body effects in multilayer-film adsorption,” *Phys. Rev. B* **38**, 987 (1988).
- [27] A Sharma and R Khanna, “Pattern formation in unstable thin liquid films,” *Phys. Rev. Lett.* **81**, 3463 (1998).
- [28] Günter Reiter, Ashutosh Sharma, Alain Casoli, Marie Odile David, Rajesh Khanna, and Philippe Auroy, “Thin film instability induced by long-range forces,” *Langmuir* **15**, 2551 (1999).
- [29] A. Vrij, “Possible mechanism for the spontaneous rupture of thin, free liquid films,” *Discuss. Faraday Soc.* **42**, 23 (1966).
- [30] Eli Ruckenstein and Rakesh K. Jain, “Spontaneous rupture of thin liquid films,” *J. Chem. Soc. Faraday Trans. II* **70**, 132 (1974).
- [31] S. Herminghaus, “Spinodal Dewetting in Liquid Crystal and Liquid Metal Films,” *Science* **282**, 916 (1998).
- [32] Vladimir S. Mitlin, “Dewetting of Solid Surface: Analogy with Spinodal Decomposition,” *J. Colloid Interface Sci.* **156**, 491 (1993).
- [33] J. S. Langer, “Theory of spinodal decomposition in alloys,” *Ann. Phys.* **65**, 53 (1971).
- [34] (2018), See Supplemental Material for more details.
- [35] Jacob N. Israelachvili, *Intermolecular and Surface Forces* (Academic Press, 2011).
- [36] M. I. Katsnelson, “Coulomb drag in graphene single layers separated by a thin spacer,” *Phys. Rev. B* **84**, 041407 (2011).
- [37] S. M. Badalyan and F. M. Peeters, “Effect of nonhomogenous dielectric background on the plasmon modes in graphene double-layer structures at finite temperatures,” *Phys. Rev. B* **85**, 195444 (2012).
- [38] Valeri N. Kotov, Bruno Uchoa, Vitor M. Pereira, F. Guinea, and A. H. Castro Neto, “Electron-electron interactions in graphene: Current status and perspectives,” *Rev. Mod. Phys.* **84**, 1067 (2012).
- [39] E.M. Lifshitz and L.P. Pitaevskii, *Statistical Physics*, Part 2 (Pergamon Press, 1980).
- [40] Lennart Bergström, “Hamaker constants of inorganic materials,” *Adv. Col. Int. Sci.* **70**, 125 (1997).
- [41] Je Luen Li, Jaehun Chun, Ned S. Wingreen, Roberto Car, Ilhan A. Aksay, and Dudley A. Saville, “Use of dielectric functions in the theory of dispersion forces,” *Phys. Rev. B* **71**, 235412 (2005).
- [42] K. I. Bolotin, K. J. Sikes, Z. Jiang, M. Klima, G. Fudenberg, J. Hone, P. Kim, and H. L. Stormer, “Ultrahigh electron mobility in suspended graphene,” *Solid State Commun.* **146**, 351 (2008).
- [43] Jannik C. Meyer, A. K. Geim, M. I. Katsnelson, K. S. Novoselov, T. J. Booth, and S. Roth, “The structure of suspended graphene sheets,” *Nature* **446**, 60 (2007).
- [44] L.D. Landau and E.M. Lifshitz, *Statistical Physics*, Part 1 (Pergamon Press, 1980).
- [45] P. G. De Gennes, “Wetting: statics and dynamics,” *Rev. Mod. Phys.* **57**, 827 (1985).
- [46] Karine Ragil, Jacques Meunier, Daniel Broseta, Joseph Indekeu, and Daniel Bonn, “Experimental Observation of Critical Wetting,” *Phys. Rev. Lett.* **77**, 1532 (1996).
- [47] Françoise Brochard-Wyart, Jean Marc di Meglio, David Quéré, and Pierre Gilles de Gennes, “Spreading of Non-volatile Liquids in a Continuum Picture,” *Langmuir* **7**, 335 (1991).
- [48] Rudolf Peierls, “Clustering in adsorbed films,” *Phys. Rev. B* **18**, 2013 (1978).
- [49] J. G. Dash, “Clustering and percolation transitions in helium and other thin films,” *Phys. Rev. B* **15**, 3136 (1977).
- [50] Volker C. Weiss, Emanuel Bertrand, Salima Rafai, Joseph O. Indekeu, and Daniel Bonn, “Effective exponents in the long-range critical wetting of alkanes on aqueous substrates,” *Phys. Rev. E* **76**, 051602 (2007).
- [51] E. Van Cleve, P. Taborek, and J. E. Rutledge, “Helium adsorption on lithium substrates,” *J. Low Temp. Phys.* **150**, 1 (2008).

Supplementary material for “Theory of liquid film growth and wetting instabilities on graphene”

Sanghita Sengupta, Nathan Nichols, Adrian Del Maestro, Valeri Kotov

In this supplement we provide additional information and details on the theory of Dzyaloshinskii-Lifshitz-Pitaevskii, the polarization function of graphene and the dielectric constants of the light gases and substrates studied in the main text. We provide complementary results for different substrates in general experimental use and present additional calculations on how the conclusions of the main text would be altered when placing the two-dimensional (2D) substrate under uniaxial strain or doping. Results for several transition-metal monolayer dichalcogenides (which exhibit energy gaps) are compared with graphene. We conclude with a technical discussion on the effects of temperature which can be safely neglected in the parameter regime of interest in the main text. In what follows, we adopt the units $\hbar = k_B = 1$.

Dzyaloshinskii-Lifshitz-Pitaevskii (DLP) theory

The DLP theory [S1, S2] is the standard many-body approach used to calculate the van der Waals forces in a substrate-liquid-vapor configuration and then relate the film thickness to pressure when analyzing experiments (Eq.(10)). Comparison with experiments on various materials [S3–S5] generally shows very good agreement, with deviations occurring in various circumstances typically attributable to presence of forces beyond long-range van der Waals (e.g. short-range forces), or the very complex nature of dielectric screening, etc. From a theoretical viewpoint DLP provides calculation of the van der Waals effective force between the two boundaries (“disjoining pressure”). It treats the dielectrics as effective homogeneous media with certain frequency-dependent dielectric functions, which themselves could be hard to calculate but are fairly well-known for standard materials after many years of comparison with experiment. The polarization loops within DLP theory are basically re-summed self-consistently in close analogy with the RPA (random phase approximation), which is the standard way to include self-consistent screening. It should also be noted that examination of different theoretical aspects of DLP theory [S1, S6, S7] shows that the approach used in the main text of the paper (based on the calculation of the effective dielectric function) is equivalent to other approaches, such as those based on determining electromagnetic fluctuations via photon Green’s functions in a medium and the van der Waals stress tensor.

Graphene Polarization and Gas Parameters

The dynamical polarization of graphene at zero chemical potential (charge neutrality point), on the imaginary frequency axis, has the form [S8]:

$$\Pi(\mathbf{q}, i\omega) = -\frac{1}{4} \frac{|\mathbf{q}|^2}{\sqrt{v^2|\mathbf{q}|^2 + \omega^2}}, \quad (\text{S1})$$

where $v = 6.6 \text{ eV } \text{\AA}$ is the velocity of the Dirac quasiparticles.

The parameters of the three light gases (medium 2) discussed in the main text are as follows (see e.g. [S9, S10]). For Helium the dynamical dielectric constant is

$$\varepsilon_2(i\omega) = 1 + 4\pi n_{\text{He}} \alpha(i\omega), \quad \alpha(i\omega) = \frac{\alpha_{\text{He}}}{1 + (\omega/\omega_{\text{He}})^2}, \quad (\text{S2})$$

where the density $n_{\text{He}} = 2.12 \times 10^{-2} \text{\AA}^{-3}$, the static polarizability $\alpha_{\text{He}} = 1.38 \text{ a.u.}$, and the characteristic oscillator frequency $\omega_{\text{He}} = 27.2 \text{ eV}$. The atomic unit of polarizability is defined as $1 \text{ a.u.} = 0.148 \text{\AA}^3$.

For Nitrogen and Hydrogen, which have densities comparable to Helium but significantly larger polarizabilities, more accurate formulas based on the Clausius-Mossotti relation are typically used:

$$\varepsilon_2(i\omega) = 1 + \frac{4\pi n_A \alpha(i\omega)}{1 - \frac{4\pi}{3} n_A \alpha(i\omega)}, \quad A = \text{N}_2, \text{H}_2, \quad (\text{S3})$$

The dynamical polarizability is defined as in Eq. (S2). For H_2 the parameters are: $n_{\text{H}_2} = 2.04 \times 10^{-2} \text{\AA}^{-3}$, $\alpha_{\text{H}_2} = 5.44 \text{ a.u.}$, $\omega_{\text{H}_2} = 14.09 \text{ eV}$. For N_2 : $n_{\text{N}_2} = 1.73 \times 10^{-2} \text{\AA}^{-3}$, $\alpha_{\text{N}_2} = 11.74 \text{ a.u.}$, $\omega_{\text{N}_2} = 19.32 \text{ eV}$.

A convenient expression for the dimensionless quantity $I(d)$ appearing in Eq. (8) is

$$I(d) = \int_0^\infty \int_0^\infty dy dx x^2 e^{-x} \frac{\varepsilon_2(y) - 1}{\varepsilon_2(y) + 1} \frac{1}{\varepsilon_2(y) + \varepsilon_3(y)} \times \left\{ \varepsilon_3(y) - \varepsilon_2(y) + \frac{4gx\varepsilon_2(y)}{[\varepsilon_2(y) + \varepsilon_3(y)] \sqrt{x^2 + y^2 [\Omega(d)]^2 + 2gx}} \right\}, \quad (\text{S4})$$

where $\Omega(d) = 2\omega_A d/v$ and $x = 2qd$. Since $\varepsilon_2(i\omega)$ is a function of the frequency ratio, $\varepsilon_2(i\omega/\omega_A)$, we define $y = \omega/\omega_A$ and use the notation $\varepsilon_2(i\omega/\omega_A) \rightarrow \varepsilon_2(y)$. In the substrate dielectric function ε_3 , see below, this leads to the rescaling $\varepsilon_3(y) = 1 + \frac{C_{IR}}{1+y^2(\omega_A/\omega_{IR})^2} + \frac{C_{UV}}{1+y^2(\omega_A/\omega_{UV})^2}$. The dimensionless coupling $g = (\pi/2)(e^2/v) \approx (\pi/2)(2.2)$ characterizes the Coulomb interaction strength in graphene in vacuum.

Substrate Effects

It is instructive to investigate the effect of different substrates (medium 3) on wetting. Many dielectric substrates are accurately described by the formula [S11]

$$\varepsilon_3(i\omega) = 1 + \frac{C_{IR}}{1 + (\omega/\omega_{IR})^2} + \frac{C_{UV}}{1 + (\omega/\omega_{UV})^2}. \quad (\text{S5})$$

As an example, we have performed calculations for 6H-SiC, see Fig. S1, to be compared with our results in Fig. 2 of the main text (for a SiO₂ substrate). While the magnitude of the van der Waals force shows significant variations between substrates, the overall distance dependence, and crossover length scale remains comparable.

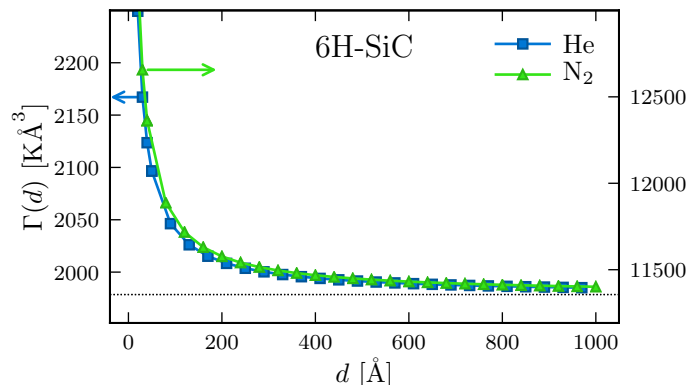


FIG. S1. Van der Waals force contribution $\Gamma(d)$ for a 6H-SiC substrate with parameters $C_{IR} = 3.67$, $\omega_{IR} = 0.1$ eV, $C_{UV} = 5.53$, $\omega_{UV} = 7.39$ eV [S11]. This can be compared with that of a SiO₂ substrate plotted as Fig. 2 of the main text.

Another important quantity which characterizes the van der Waals force is the length scale L defined in Eq. (9) which sets the crossover from $1/d^3$ to $1/d^4$ behavior. Due to the Dirac fermion motion in graphene (i.e. the strong momentum dependence of graphene's polarization) the force crosses over to a stronger power law at distances beyond L . In Fig. S2 we present a general analysis of the substrate dependence of L , for He. Due to helium's large atomic frequency $\omega_{He} \approx 27$ eV, it is easy to see that only the ultraviolet (UV) part in Eq. (S5) provides an important contribution to the relevant integral, while the infrared (IR) part is irrelevant. Our results can be used to characterize a variety of substrates [S11], beyond the two main ones studied in this work. It is important to notice that L remains fairly small (several Å) for practically all available substrates.

Influence of Uniaxial Strain in Graphene

The existence of two-dimensional (2D) materials such as graphene opens up the attractive possibility to manipulate van der Waals forces by mechanical manipulation of the substrate – strain. This is due to the strong influence of

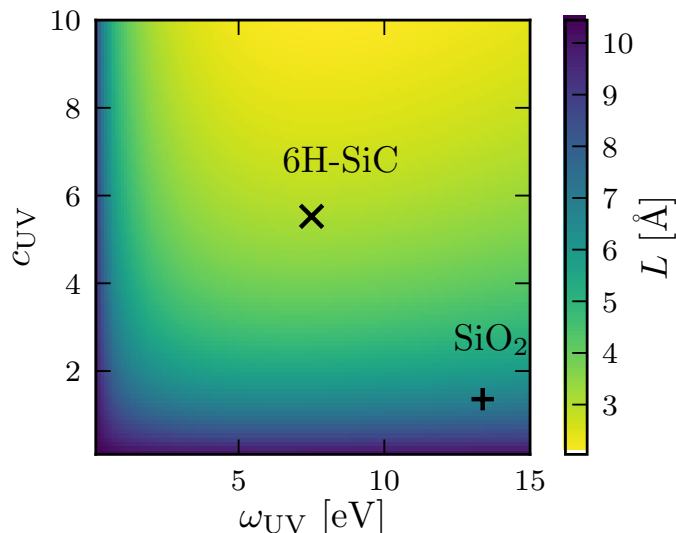


FIG. S2. Map of the crossover length L for He, defined in Eq. (9), as a function of the two main substrate parameters.

strain on the electronic motion and consequently substantial change in graphene's polarization [S12, S13]. The case of uniaxial strain is the most straightforward to analyze, in which case graphene's polarization is

$$\Pi(\mathbf{q}, i\omega) = -\frac{1}{4v_x v_y} \frac{v_x^2 q_x^2 + v_y^2 q_y^2}{\sqrt{v_x^2 q_x^2 + v_y^2 q_y^2 + \omega^2}}. \quad (\text{S6})$$

Here we assume strain is in the y (armchair) direction leading to decrease of the electron velocity v_y in that direction (while the velocity in the perpendicular (x) direction remains practically unchanged). It is convenient to introduce the ratio $v_\perp = v_y/v_x < 1$ which reflects the strain (relative increase in lattice spacing); this ratio is perturbatively proportional to strain for small values but exhibits non-linear behavior for larger deformations [S12, S13]. For example $v_\perp = 0.2$ corresponds to 34% strain, $v_\perp = 0.4$ corresponds to 25% strain, and $v_\perp = 0.75$ corresponds to 10% strain.

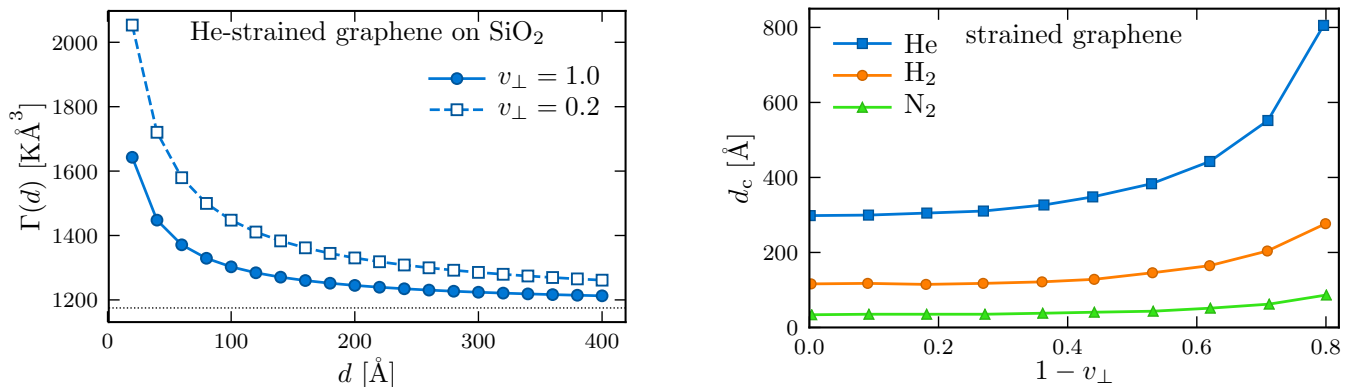


FIG. S3. Left: Influence of strong (for illustrative purposes) graphene strain ($v_y/v_x = 0.2$, 34% strain) for He on SiO_2 substrate, leading to significant enhancement of the van der Waals force. The value $v_y/v_x = 1$ corresponds to isotropic, unstrained graphene. Right: Strain dependence of critical film thickness d_c in the suspended graphene geometry. For example the parameter value $1 - v_\perp = 0.8$ corresponds to 34% strain, while $1 - v_\perp = 0.6$ corresponds to 25% strain. The general tendency, particularly important for moderate to strong strain, is promotion of film growth (increase of critical d_c).

Figure S3 quantifies the effects of strain. Due to the increase of the graphene polarization Eq. (S6), the van der Waals interaction increases and thus strain promotes wetting. While at present such strong strain is difficult to achieve

in graphene, mechanical deformations are also expected to be present in a variety of 2D materials [S14], and thus the general tendencies described here could be important in a variety of physical situations.

As a consequence of the enhanced van der Waals interaction with strain, the tendency towards film growth is enhanced. In particular, while in the suspended geometry (suspended graphene with no supporting substrate) films can grow only up to a finite thickness d_c , the value of d_c increases with strain as illustrated in Fig. S3 (right). This effect is quite weak for small strain and becomes significant as strain grows. In addition we find substantial dependence on the type of atom (the effect is strongest for helium).

2D Materials: Insulating Dichalcogenides and Doped Graphene

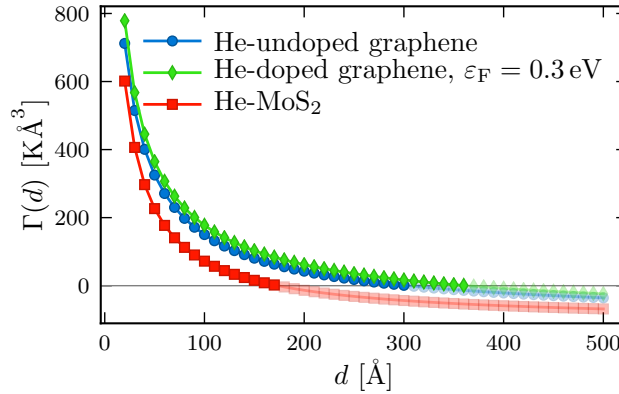


FIG. S4. Variation of the van der Waals force $\Gamma(d)$ in the case of He in the suspended geometry: MoS₂ compared to doped and undoped graphene. The result shows significant decrease of the maximum film thickness d_c (from 300Å to ≈ 180 Å), caused by the suppression of the force due to the presence of the large electronic gap Δ in MoS₂. A representative (quite substantial) doping value is also shown to illustrate the tendency with doping. The shown value of ε_F corresponds to graphene carrier density $n_e \approx 7 \times 10^{12} \text{ cm}^{-2}$, well above the lowest-possible density that can be achieved in suspended graphene ($\approx 10^{9-10} \text{ cm}^{-2}$). More detailed variation with density appears on the next figure.

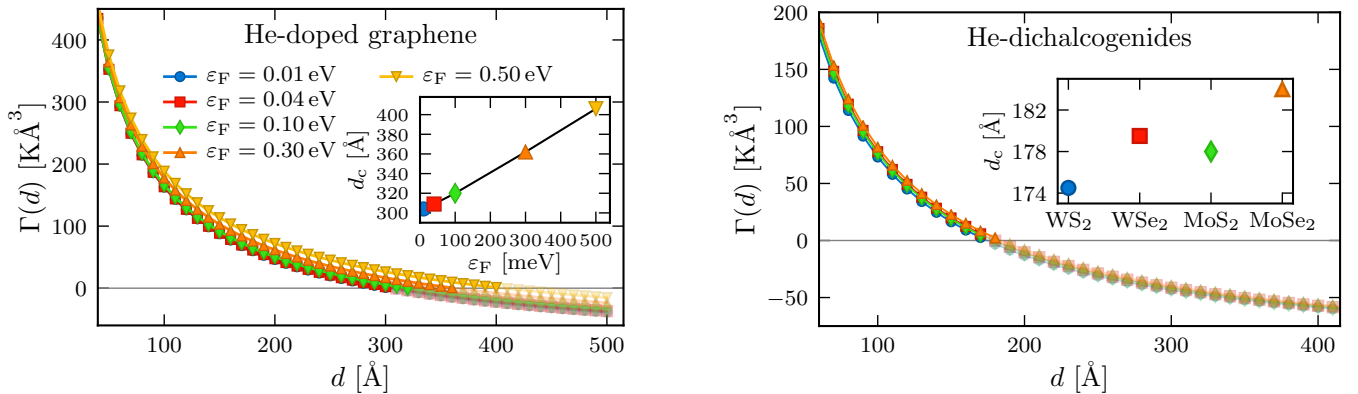


FIG. S5. Left: Variation of the van der Waals force $\Gamma(d)$ in the case of He in the suspended geometry, for doped graphene. The densities corresponding to the shown Fermi energies are: $n_e \approx 8 \times 10^9, 10^{11}, 10^{12}, 7 \times 10^{12}, 2 \times 10^{13} \text{ cm}^{-2}$. For smaller densities ($\varepsilon_F < 40 \text{ meV}$) the results are indistinguishable from the undoped situation. The Fermi energy is related to the density via $\varepsilon_F = v\sqrt{\pi n_e}$. The overall effect of doping is quite small and becomes noticeable for higher densities only. The general tendency is an increase of d_c due to the increased polarization of doped graphene (inset). Right: Comparison of various members of the dichalcogenides family, showing remarkably similar behavior. The material parameters, Δ – gap, v – velocity, $g = (\pi/2)e^2/v$ – Coulomb interaction, are: WS₂: $\Delta = 1.79 \text{ eV}$, $v = 4.38 \text{ eV \AA}$, $g = 5.16$; WSe₂: $\Delta = 1.6 \text{ eV}$, $v = 3.94 \text{ eV \AA}$, $g = 5.74$; MoS₂: $\Delta = 1.66 \text{ eV}$, $v = 3.51 \text{ eV \AA}$, $g = 6.44$; MoSe₂: $\Delta = 1.47 \text{ eV}$, $v = 3.11 \text{ eV \AA}$, $g = 7.26$.

Dichalcogenides. While graphene provides the most well studied example of a 2D material, it is important to assess the applicability of our results to other 2D compounds. Numerous 2D materials have been discovered, forming groups suitable for designing so-called van der Waals heterostructures [S15]. In particular the group-VI dichalcogenides [S16] include e.g. MoS₂, WS₂, MoSe₂, etc., which exhibit a significant electronic gap Δ of order 1 eV, as well as a small spin-orbital interaction. For the purpose of van der Waals calculations, the most significant modification (compared to graphene) to be taken into account is the presence of the gap, while the spin-orbital component can be neglected. The polarization function in this case is [S17]

$$\Pi(\mathbf{q}, i\omega) = -\frac{|\mathbf{q}|^2}{\pi} \left[\frac{m}{\tilde{q}^2} + \frac{1}{2\tilde{q}} \left(1 - \frac{4m^2}{\tilde{q}^2} \right) \tan^{-1} \left(\frac{\tilde{q}}{2m} \right) \right], \quad \tilde{q} \equiv \sqrt{v^2|\mathbf{q}|^2 + \omega^2}, \quad m = \Delta/2, \quad (\text{S7})$$

where m is the Dirac mass (half of electronic gap). For example for MoS₂ $\Delta = 1.66$ eV, and other materials have similar parameters [S16]. Neglecting the small spin-orbit interaction can result in several percent error but our main conclusions will remain intact. We assume materials are in their insulating phases, i.e. the Fermi energy is in the gap.

We consider the wetting instability in the suspended geometry, as was done for graphene in the main text (Figure 3). The main effect of the gap is the suppression of the van der Waals force. Consequently this causes a significant enhancement of the instability (film growth arrested at smaller thickness $d = d_c$) as shown in Fig. S4 for MoS₂, to be compared with results for graphene in Figure 3 of the main text. Results for other dichalcogenides are similar and summarized in Fig. S5 (right). Therefore the critical wetting instability is present in the four main members of the dichalcogenides family, with very similar values of the critical film thickness d_c .

Doped Graphene. It is also important to investigate the effect of finite carrier concentration n_e in graphene, when the Fermi energy ε_F is shifted away from the Dirac (charge neutrality) point, and compare with results for undoped graphene ($\varepsilon_F = 0$). Experimentally, in suspended graphene samples [S18, S19], the carrier density can be very small $n_e < 10^{10}$ cm⁻², and thus a close proximity to the Dirac point can be achieved, with $\varepsilon_F \sim 10$ meV.

We use the well-known polarization for doped graphene [S20]

$$\Pi(\mathbf{q}, i\omega) = -\frac{q^2}{4\sqrt{\omega^2 + v^2q^2}} - \frac{2\varepsilon_F}{\pi v^2} + \frac{q^2}{2\pi\sqrt{\omega^2 + v^2q^2}} \Re e \left[\arcsin \left(\frac{2\varepsilon_F + i\omega}{vq} \right) + \left(\frac{2\varepsilon_F + i\omega}{vq} \right) \sqrt{1 - \left(\frac{2\varepsilon_F + i\omega}{vq} \right)^2} \right] \quad (\text{S8})$$

and our results are summarized in Fig. S5 (left). It is clear that at small densities the results for doped and undoped graphene are practically identical. Significant modification of d_c starts appearing only in the regime $\varepsilon_F > 100$ meV, which corresponds to substantial density $n_e \gtrsim 10^{12}$ cm⁻². It is natural that the instability tends to become suppressed with doping (i.e. d_c tends to increase) since the polarization of graphene in the metallic regime increases. However we can confidently conclude that in the low-density regime, easily achievable in suspended graphene samples, our results discussed in the main body of the paper remain practically unchanged. In addition, the critical wetting instability also remains fully present in strongly-doped suspended graphene (Fig. S5 (left).)

Overall we conclude that the instability in the suspended geometry, with d_c within several hundred Angstroms, is present in all three main 2D Dirac material groups: (insulating) dichalcogenides, semi-metallic (undoped) graphene, and doped graphene. Figure S4 summarizes the main tendencies exhibited by representatives of those groups, namely an increase of the critical film thickness as systems transition from insulating to metallic behavior.

Effect of Temperature

The instability in the suspended graphene geometry is essentially a zero temperature phenomenon, since we work in the temperature range where the light elements we consider form a liquid (e.g. $T \approx 2$ K for He, and somewhat higher $T \approx 20$ K for H₂). In fact we can readily see that the effect of temperature at the distances involved in any of our geometries (up to several hundred Angstroms) is negligible. Indeed, the basic expressions Eqs. (6-7) of the main text have the following form, which we now write in the finite temperature formalism, introducing the Matsubara frequencies ω_m (the prime means that the zero frequency term should be divided by two)

$$T \sum'_m \left(f_1(i\omega_m) + f_2(i\omega_m) \frac{e^{2\Pi(q, i\omega_m)}}{q} \right), \quad \omega_m = 2\pi mT. \quad (\text{S9})$$

Here we have written explicitly only the frequency sums, not showing the momentum integrations (weighted by the exponential factors e^{-2qd}). The function $f_1(i\omega_m) \sim [\varepsilon_2(i\omega_m) - 1]^2$ in the suspended geometry ($\varepsilon_3 = 1$), while

$f_1(i\omega_m) \sim [\varepsilon_2(i\omega_m) - 1]$ in the other geometries with substrates present. This is the purely dielectric part. In the second term, involving graphene, we have $f_2(i\omega_m) \sim [\varepsilon_2(i\omega_m) - 1]$, proportional to the atomic polarizability. There exist other combinations of substrate dielectric screening factors within these two functions but we do not write them explicitly since it is easy to see that their existence is harmless and does not change the arguments that follow.

In the first term, since the dielectric function enters via the frequency ratio ω_m/ω_A (Eq. (S2)), i.e. the combination $T/\omega_A \ll 1$, it is evident that the sum transforms into the zero temperature frequency integration. Recall that $\omega_A \sim 10\text{eV} \sim 10^5\text{K}$.

In the second term, the characteristic momentum is of order $q = q^* \sim 1/d$ (which is the momentum where the integral over q accumulates due to the presence of the exponential factor). Taking into account that Π has the form Eq. (S1) it is clear that as long as $T \ll v/d$, the sum is essentially at zero temperature. One should keep in mind that: (I) This condition is satisfied up to distances of several hundred Angstroms, e.g. $v/d \approx 150\text{K}$ at $d = 500\text{\AA}$, and the ratio increases at smaller distances, (II) the polarization itself has a finite T contribution, i.e. is of the form $\Pi(\mathbf{q}, i\omega_m) + \Pi_T(\mathbf{q}, i\omega_m)$, where $\Pi_T(\mathbf{q}, i\omega_m)$ can be found explicitly [S21]. Calculations that take into account the full temperature dependence of the polarization confirm the above estimates and show that indeed the corrections are small and certainly negligible up to several hundred \AA .

To summarize, our main conclusions, especially concerning the instability leading to finite film thickness $d_c \lesssim 400\text{\AA}$ as shown in Figures 3-4 of the main text, remain valid at finite (but small) temperatures which is the regime of interest for liquid phases of light elements. At larger distances, finite temperature as well as relativistic corrections will gradually become more pronounced.

-
- [S1] I.E. Dzyaloshinskii, E.M. Lifshitz, and L.P. Pitaevskii, “The general theory of van der Waals forces,” *Adv. in Phys.* **10**, 165 (1961).
- [S2] I.E. Dzyaloshinskii, E.M. Lifshitz, and L.P. Pitaevskii, “van der Waals Forces in Liquid Films,” *Sov. Phys. JETP* **37**, 161 (1960).
- [S3] E. S. Sabisky and C. H. Anderson, “Verification of the Lifshitz Theory of the van der Waals Potential Using Liquid-Helium Films,” *Phys. Rev. A* **7**, 790 (1973).
- [S4] V. Panella, R. Chiarello, and J. Krim, “Adequacy of the Lifshitz Theory for Certain Thin Adsorbed Films,” *Phys. Rev. Lett.* **76**, 3606–3609 (1996).
- [S5] Jacob N. Israelachvili, *Intermolecular and Surface Forces* (Academic Press, 2011).
- [S6] Yurii S. Barash and Vitalii L. Ginzburg, “Electromagnetic fluctuations in matter and molecular (Van-der-Waals) forces between them,” *Sov. Phys. Usp.* **18**, 305 (1975).
- [S7] E.M. Lifshitz and L.P. Pitaevskii, *Statistical Physics*, Part 2 (Pergamon Press, 1980).
- [S8] Valeri N. Kotov, Bruno Uchoa, Vitor M. Pereira, F. Guinea, and A. H. Castro Neto, “Electron-electron interactions in graphene: Current status and perspectives,” *Rev. Mod. Phys.* **84**, 1067 (2012).
- [S9] E. Cheng and Milton W. Cole, “Retardation and many-body effects in multilayer-film adsorption,” *Phys. Rev. B* **38**, 987 (1988).
- [S10] Susanna Rauber, James R. Klein, Milton W. Cole, and L. W. Bruch, “Substrate-mediated dispersion interaction between adsorbed atoms and molecules,” *Surf. Sci.* **123**, 173 (1982).
- [S11] Lennart Bergström, “Hamaker constants of inorganic materials,” *Adv. Col. Int. Sci.* **70**, 125 (1997).
- [S12] Nathan S. Nichols, Adrian Del Maestro, Carlos Wexler, and Valeri N. Kotov, “Adsorption by design: Tuning atom-graphene van der Waals interactions via mechanical strain,” *Phys. Rev. B* **93**, 205412 (2016).
- [S13] Anand Sharma, Peter Harnish, Alexander Sylvester, Valeri N Kotov, and A H Castro Neto, “van der Waals forces and electron-electron interactions in two strained graphene layers,” *Phys. Rev. B* **89**, 235425 (2014).
- [S14] B Amorim, A Cortijo, F de Juan, A G Grushin, F Guinea, A Gutiérrez-Rubio, H Ochoa, V Parente, R Roldán, P San-Jose, J Schiefele, M Sturla, and M A H Vozmediano, “Novel effects of strains in graphene and other two dimensional materials,” *Phys. Rep.* **617**, 1 (2016).
- [S15] K. S. Novoselov, A. Mishchenko, A. Carvalho, and A. H. Castro Neto, “2D materials and van der Waals heterostructures,” *Science* **353** (2016), 10.1126/science.aac9439.
- [S16] Di Xiao, Gui Bin Liu, Wanxiang Feng, Xiaodong Xu, and Wang Yao, “Coupled Spin and Valley Physics in Monolayers of MoS₂ and Other Group-VI Dichalcogenides,” *Phys. Rev. Lett.* **108**, 196802 (2012).
- [S17] Valeri N Kotov, Vitor M Pereira, and Bruno Uchoa, “Polarization charge distribution in gapped graphene: Perturbation theory and exact diagonalization analysis,” *Phys. Rev. B* **78**, 75433 (2008).
- [S18] D. C. Elias, R. V. Gorbachev, A. S. Mayorov, S. V. Morozov, A. A. Zhukov, P. Blake, L. A. Ponomarenko, I. V. Grigorieva, K. S. Novoselov, F. Guinea, and A. K. Geim, “Dirac cones reshaped by interaction effects in suspended graphene,” *Nature Physics* **8**, 172 (2012).
- [S19] Xu Du, Ivan Skachko, Anthony Barker, and Eva Andrei, “Approaching ballistic transport in suspended graphene,” *Nature Nanotechnology* **3**, 491 (2008).
- [S20] Yafis Barlas, T. Pereg-Barnea, Marco Polini, Reza Asgari, and A. H. MacDonald, “Chirality and correlations in graphene,”

Phys. Rev. Lett. **98**, 236601 (2007).

- [S21] G. L. Klimchitskaya and V. M. Mostepanenko, “Origin of large thermal effect in the Casimir interaction between two graphene sheets,” Phys. Rev. B **91**, 174501 (2015).